

Spatio-seasonal risk assessment of upward lightning at tall objects using meteorological reanalysis data

Isabell Stucke^{1,2}, Deborah Morgenstern^{1,2}, Gerhard Diendorfer³, Georg J. Mayr², Hannes Pichler³, Wolfgang Schulz³, Thorsten Simon⁴, Achim Zeileis¹

¹Institute of Statistics, University of Innsbruck, Austria, Innsbruck

²Institute of Atmospheric and Cryospheric Sciences, University of Innsbruck, Austria, Innsbruck

³OVE Service GmbH, Dept. ALDIS (Austrian Lightning Detection & Information System), Austria, Vienna

⁴Department of Mathematics, University of Innsbruck, Austria, Innsbruck

Key Points:

- Strong winds near the surface and upward deflection by obstructing terrain increase the risk of upward lightning at tall objects.
- Lightning at tall wind turbines can account for up to 20 % of total lightning activity north of the Alps.
- High-risk areas are north and east of the Alps in winter and shift southward in the transition seasons and summer.

Abstract

This study investigates lightning at tall objects and evaluates the risk of upward lightning (UL) over the eastern Alps and its surrounding areas. While uncommon, UL poses a threat, especially to wind turbines, as the long-duration current of UL can cause significant damage. Current risk assessment methods overlook the impact of meteorological conditions, potentially underestimating UL risks. Therefore, this study employs random forests, a machine learning technique, to analyze the relationship between UL measured at Gaisberg Tower (Austria) and 35 larger-scale meteorological variables. Of these, the larger-scale upward velocity, wind speed and direction at 10 meters and cloud physics variables contribute most information. The random forests predict the risk of UL across the study area at a 1 km² resolution. Strong near-surface winds combined with upward deflection by elevated terrain increase UL risk. The diurnal cycle of the UL risk as well as high-risk areas shift seasonally. They are concentrated north/northeast of the Alps in winter due to prevailing northerly winds, and expanding southward, impacting northern Italy in the transitional and summer months. The model performs best in winter, with the highest predicted UL risk coinciding with observed peaks in measured lightning at tall objects. The highest concentration is north of the Alps, where most wind turbines are located, leading to an increase in overall lightning activity. Comprehensive meteorological information is essential for UL risk assessment, as lightning densities are a poor indicator of lightning at tall objects.

Plain Language Summary

This study investigates the risk of upward lightning (UL) in the eastern Alps and surrounding regions, which is critical for tall objects such as wind turbines. Current risk assessments often overlook meteorological conditions, potentially underestimating the hazard. Using random forests, a machine learning method, the study analyzes UL at the Gaisberg Tower in Austria, taking into account 35 meteorological factors. Key contributors include wind speed, wind direction, and cloud physics. The model predicts UL risk at a resolution of 1 km², highlighting higher-risk areas influenced by near-surface winds and terrain. Risk varies daily and seasonally, peaking in winter north of the Alps and shifting southward in warmer months. Winter predictions are consistent with observed lightning at tall objects, particularly concentrated north of the Alps where wind turbines are prevalent. This study highlights the importance of detailed meteorological data for accurate UL risk assessment and demonstrates that general lightning densities are inadequate indicators of the safety of tall objects.

1 Introduction

Wind power has become the cornerstone of the transition to a greener and more sustainable future. This transition is being driven by the continued expansion of wind turbines as well as by investments to extend the life time of existing facilities. The sensitive turbines are exposed not only to the wind that generates the electricity, but also to various other forces of nature. Among these natural forces, lightning has gained particular attention in recent years (e.g., IEC 61400-24, 2019; Candela Garolera et al., 2016; Montanyà et al., 2016). Depending on both the physical height of the turbine and its elevation relative to the surrounding terrain, it can be exposed to a strong amplification of the electric field. This amplification is often expressed in terms of the effective height. The effective height is larger if a tall object is located on a mountain or hill (e.g., Zhou et al., 2010; Shindo, 2018). For objects with effective heights below about 100 m, the main proportion of lightning at tall objects is assumed to be downward lightning (DL). For objects with an effective height greater than 100 m, a critical proportion of lightning can be upward lightning (UL). UL only initiates from tall objects and propagates upward

67 towards the charged thundercloud. For objects with effective heights greater than 500
68 m, all lightning is assumed to be UL (Rakov & Uman, 2003).

69 Although rare, UL may cause considerable damage to wind turbines. A particu-
70 larly prolonged current flow can transfer large amounts of charge, which can lead to the
71 melting of individual rotor blades or even the complete failure of the turbine (e.g., Birkl
72 et al., 2017). The lightning receptors installed at the tip of the Gaisberg Tower in Salzburg
73 (Austria) reveal that, unlike DL, UL is relatively evenly distributed throughout the year,
74 with a slight preference for the colder seasons (Diendorfer et al., 2009). Better under-
75 standing and predicting these rare events, as well as a better risk assessment, is essen-
76 tial for extending the life of individual existing or planned wind turbines, e.g., by equip-
77 ping them with appropriate lightning protection devices (IEC 61400-24, 2019).

78 The most serious problem in a spatio-temporal risk assessment is the lack of nec-
79 cessary data. The UL observations at the Gaisberg Tower show that more than 50 % of
80 UL never appear in the data of conventional lightning location systems (LLS). This is
81 because conventional LLS cannot detect a particular subtype of UL that does not emit
82 an electromagnetic field strong enough to be detectable and consists only of a long du-
83 ration initial continuous current (ICC) (Diendorfer et al., 2015). The result is a critical
84 underestimation of the actual UL activity and therefore of total lightning at tall objects.
85 As LLS do not distinguish between UL and DL, in the current study lightning at tall ob-
86 jects may include both DL and UL from an effective height ≥ 100 m.

87 Current standards to assess the risk of lightning at wind turbines incorporate tech-
88 nical and topographical features, focusing on three key elements. These include the den-
89 sity of lightning strikes per square kilometer annually, the height of the wind turbine rep-
90 resented by its circular collection area (with a radius three times its height), and a spe-
91 cific environmental factor (IEC 61400-24, 2019; Rachidi et al., 2008; Pineda et al., 2018;
92 March, 2018). However, challenges arise in this assessment. The local annual lightning
93 density predominantly considers lightning during the convective warm season when they
94 peak annually, largely overlooking lightning during other seasons and particularly UL,
95 which studies suggest pose a significant threat to wind turbines year-round (e.g., Becerra
96 et al., 2018). Since UL results from complex atmospheric processes acting on different
97 scales, it is crucial to recognize the significant impact of meteorological conditions. Ne-
98 glecting these factors might lead to a substantial underestimation of the risk posed by
99 lightning at tall objects, particularly by UL.

100 Investigating the rare and underrated phenomenon using unique UL observations
101 at the Gaisberg Tower in combination with a wide range of globally available atmospheric
102 reanalysis variables using flexible machine learning techniques offers a great opportunity
103 for better risk assessment compared to the current standards. Machine learning can not
104 only compensate for the problem of missing data, but also provide meaningful insights,
105 recognize patterns and achieve better predictability.

106 The study consists of two main steps. In the first step, random forests based on
107 data from the Gaisberg Tower are used to learn which larger-scale meteorological vari-
108 ables are responsible for triggering UL. The tower-trained models are then applied to a
109 larger study area, including Austria, southern and central Germany, Italy, and Switzer-
110 land, to obtain high-resolution (1 km^2) seasonal and annual UL risk maps for the en-
111 tire area. In order to better understand the predicted risk, the seasonal variations of the
112 most influential larger-scale meteorological variables found at the Gaisberg Tower are
113 investigated. LLS-observed lightning at objects (not just at wind turbines) with an ef-
114 fective height ≥ 100 m are used to verify the resulting risk maps.

2 Data

The study requires meteorological data, lightning data and a database of all tall objects within a chosen study area comprised of flat, hilly and complex terrain in the eastern Alps (Fig. 1). Larger-scale reanalysis data (ERA5) with hourly resolution (Hersbach et al., 2020) form the basis of all meteorological investigations in this study. In addition, ground-truth lightning current measurements at the Gaisberg Tower in Salzburg (Austria, Diendorfer et al., 2009) and LLS data from the European Cooperation for Lightning Detection (EUCLID, Schulz et al., 2016) are used. In order to verify the predicted risk at tall objects, different types of tall objects documented by the national aviation safety authorities of Austria, Switzerland, Germany and Italy are employed (ENAV Group, n.d.; Austro Control, n.d.; Swiss Federal Spatial Data Infrastructure, n.d.; Deutsche Flugsicherung, n.d.). The verification period covers three years (2021–2023).

2.1 Atmospheric reanalysis

ERA5 is the fifth generation of global climate reanalysis provided by the European Centre for Medium-Range Weather Forecasts (ECMWF). Data are available at hourly resolution and at a spatial resolution of 31 km horizontally ($0.25^\circ \times 0.25^\circ$ latitude-longitude grid) and at 137 levels vertically. Given that a precise risk assessment may necessitate a higher resolution than that offered by ERA5, the ERA5 variables are bilinearly interpolated to a $0.01^\circ \times 0.01^\circ$ latitude-longitude grid, roughly equivalent to $1 \text{ km} \times 1 \text{ km}$. In this study, 35 different variables from ERA5 are used to explain the occurrence of UL. These are either directly available or derived from variables at the surface, on model levels, or integrated vertically. A complete list of the variable groups and individual variables can be found in the supporting information.

Atmospheric reanalysis data are first used in the modeling step, where each variable is spatially and temporally interpolated to each UL observation at Gaisberg Tower. They are secondly used in the transfer step to the larger study domain shown in Fig. 1, where each variable is bilinearly interpolated to each 1 km^2 grid cell within the chosen study area in a verification period between 2021 and 2023.

2.2 Lightning measurements

LLS measurements for the study area (45°N – 50°N and 8°E – 17°E) are from the LLS EUCLID. The LLS measures at a frequency range from 400 Hz to 400 kHz and quantifies lightning flash activity with a median location accuracy of about 100 m (Schulz et al., 2016; Diendorfer, 2016; Vergeiner et al., 2013). While the LLS detects DL with a detection efficiency of more than 90 %, the detection efficiency drops to less than 50 % in the case of UL. Therefore, the proportion of UL can significantly affect the detection efficiency of lightning at tall objects.

The fundamental data source for constructing models to understand the occurrence of UL is only accessible through direct measurements on specifically instrumented towers. With a physical height of 100 m above ground and 1,288 m above mean sea level ($47^\circ 48' \text{ N}$, $13^\circ 60' \text{ E}$, Fig. 1), Gaisberg Tower predominantly experiences UL (Diendorfer et al., 2011). In total, 956 UL flashes were recorded at the Gaisberg Tower between 2000 and 2015 and from mid-2020 to the end of 2023.

Equipped with a sensitive shunt-type sensor, Gaisberg Tower measures all UL flashes, irrespective of the current waveform. Three distinct current waveforms are observed at Gaisberg Tower (Diendorfer et al., 2009). The first type emerges when the lightning process ends after the initial phase, involving only a prolonged ICC (ICC_{only}). The second type involves this ICC being overlaid with pulse type currents with relative peaks $\geq 2 \text{ kA}$ (ICC_P). Lastly, the third type of UL evolves after a brief phase of no current followed

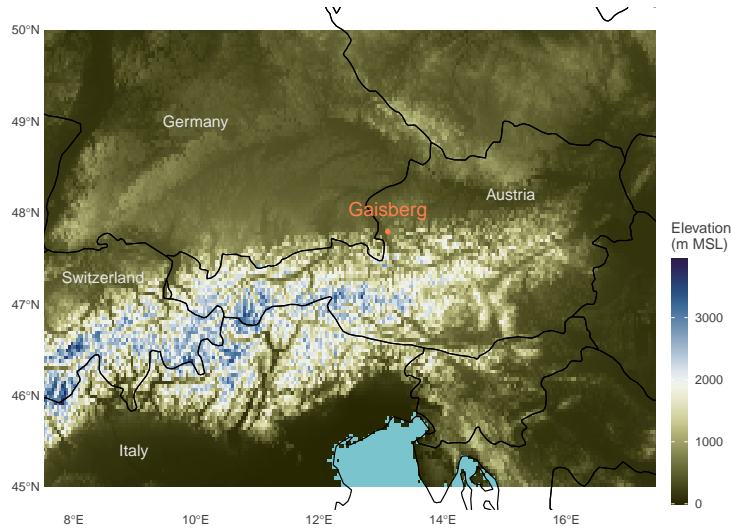


Figure 1: Topographic overview of study area and location of the instrumented Gaisberg Tower (Salzburg, Austria). Colors indicates the elevation above mean sea level according to data taken from the Shuttle Radar Topography Mission with a 90 m spatial resolution (Farr & Kobrick, 2000).

163 by one or more downward leader-upward-return stroke processes similar to those observed
 164 in DL processes (ICC_{RS}).

165 The measurements at the Gaisberg Tower showed that the ICC_{only} subtype cannot
 166 be detected by LLS at all. According to Diendorfer et al. (2015), the other two sub-
 167 types of UL presented, (ICC_{RS}) and (ICC_P), are detected by LLS in 96 % and 58 % of
 168 the cases, respectively. In order to better verify the resulting models, all analyses in this
 169 study are based exclusively on UL that can be detected by LLS, i.e., UL of the ICC_{RS}
 170 and the ICC_P type.

171 2.3 Lightning at tall objects

172 Fortuitously, international aviation regulations require each country to keep and
 173 update a database of tall objects that might endanger flight safety. The study area
 174 contains several objects with heights significant for aviation safety (see Table 1). This doc-
 175 umentation is freely available for Germany, Austria, Switzerland and Italy, but does not
 176 include data from the Czech Republic, Slovenia, Hungary and Croatia. The available database
 177 gives precise details of the geographic location and physical height of each object, pro-
 178 viding a basis for verifying the models from Sect. 3.1. Each country is based on a dif-
 179 ferent database with different levels of detail, e.g., tall trees are included in the Swiss database
 180 but not in the others.

181 UL becomes important only from an effective height of 100 m of the object (e.g.,
 182 Rakov & Uman, 2003). Hence, the verification process shall extract all LLS-observed light-
 183 ning that hit an object with an effective height ≥ 100 m between 2021 and 2023. To match

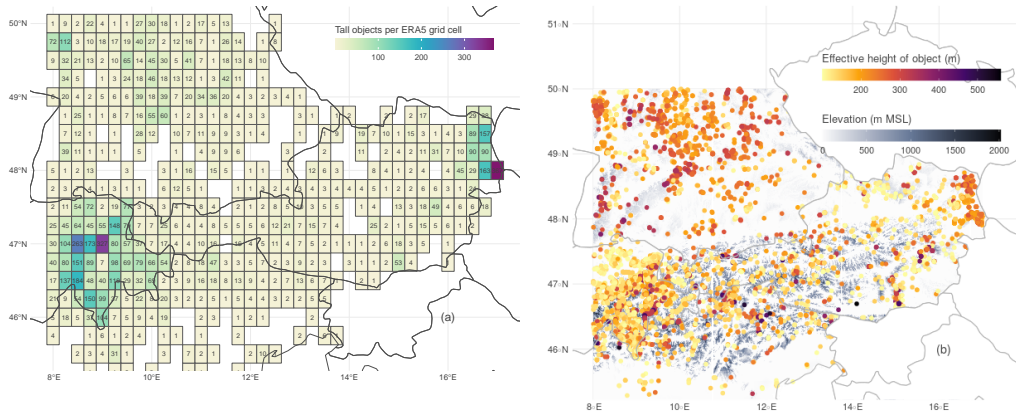


Figure 2: Panel a: accumulated number of objects with effective heights ≥ 100 m in ERA5 grid cells ($0.25^\circ \times 0.25^\circ$). Panel b: all objects with effective heights ≥ 100 m coded by color.

184 the location accuracy of LLS, all lightning within a radius of 100 meters around each ob-
 185 ject are considered (Diendorfer, 2016; Soula et al., 2019).

186 The effective height considers the difference between the height of the object above
 187 mean sea level and the height of the surrounding environment. This adjustment to the
 188 effective physical height accounts for the electric field enhancement when the mean ter-
 189 rain elevation is significantly lower than the elevation at which an object is located, such
 190 as when it is on a mountain or hill. The greater this difference, the greater the effective
 191 height and possibly the greater the proportion of total lightning at tall objects.

192 Several methods have been proposed to compute the effective height. This study
 193 uses the method described in Zhou et al. (2010), which assumes that the mountain is hemi-
 194 spherical with a height equal to the difference between the elevation of where the tall ob-
 195 ject stands and the average elevation in 1 km^2 around it. The method uses electrical field
 196 parameters derived mainly from laboratory experiments. More details are found in Zhou
 197 et al. (2010) and in the supplemental information. While this method is readily computable
 198 with the information available, it might underestimate the true effective height (Smorgonskiy
 199 et al., 2012).

200 Figure 2a gives an overview how tall objects are distributed over the study area
 201 and panel b illustrates the distribution of the effective height (≥ 100 m) of objects, rep-
 202 resented by varying colors.

203 The highest concentration of tall objects is observed in the easternmost part of Aus-
 204 tria and the central-eastern subarea of Switzerland. There are also some areas in cen-
 205 tral Germany with an increased number of tall objects. Interestingly, despite the rela-
 206 tively flat terrain in the German subarea, objects exhibit a comparatively large effective
 207 height in contrast to more mountainous terrain (panel b). This phenomenon may be at-
 208 tributed to the hilly terrain in the German subarea. In complex terrain, where moun-
 209 tains dominate the landscape, the mean elevation at the area of 1 km^2 is relatively high.
 210 Conversely, in hilly terrain, the mean elevation is relatively low, causing hills to stand
 211 significantly above the environmental average.

Table 1: List of objects in the national regions of the study area documented by the respective aviation authorities. Listed are the numbers of objects with an effective height ≥ 100 m and physical height ≥ 100 m (in parenthesis).

Type of object	Austria	German sub-area	Italian sub-area	Swiss sub-area
Wind turbine	1318 (1283)	1638 (1632)	8 (8)	17 (11)
Mast (e.g., antenna, tower)	270 (26)	166 (129)	35 (35)	90 (12)
Building	35 (35)	13 (11)	14 (5)	25 (5)
Stack	26 (26)	75 (75)	30 (30)	2 (2)
Transmission line	97 (85)	7 (7)	75 (75)	1862 (1216)
Cable car	169 (119)	1 (1)	265 (90)	520 (287)
Catenary	61 (16)	45 (45)	-	1169 (566)
Others (e.g., vegetation, bridge)	15 (15)	12 (3)	23 (15)	30 (12)
Total	1991	1957	450	3715
Total per km ²	0.024	0.024	0.009	0.17

212 3 Methods

213 First, the relationship between UL events and the larger-scale meteorology is an-
 214 alyzed using random forests, linking direct UL measurements from the Gaisberg Tower
 215 to meteorological reanalysis data. Gaisberg Tower is the only location in the study area
 216 where all types of UL are measured. The random forests are subsequently applied to the
 217 study area and evaluated with LLS-observed lightning at tall objects.

218 3.1 Model construction based on Gaisberg Tower data

219 To link meteorological reanalysis data with the occurrence of UL at the Gaisberg
 220 Tower, this study uses random forests, which is a flexible machine learning technique able
 221 to tackle nonlinear effects (Breiman, 2001).

222 Whether or not UL occurs at Gaisberg Tower is a binary classification problem.
 223 In this classification problem, 35 larger-scale meteorological variables are the predictors
 224 chosen to explain the response. The response is LLS-detectable UL at Gaisberg Tower
 225 (1) or no (LLS-detectable) UL (0) at Gaisberg Tower. Each of the meteorological vari-
 226 ables is spatio-temporally interpolated to an UL observation at Gaisberg Tower. Exclud-
 227 ing LLS undetectable UL (ICC_{only}), 549 UL observations are recorded at Gaisberg Tower.

228 The algorithm constructs decision trees by assessing the connection between the
 229 binary response and each predictor variable through permutation tests, also known as
 230 conditional inference (Strasser & Weber, 1999). At each recursive step of tree construc-
 231 tion, the predictor variable exhibiting the highest (most significant) association with the
 232 response variable is chosen. Subsequently, the dataset is partitioned based on this se-
 233 lected predictor variable to optimize the separation of different response classes. This
 234 splitting procedure is recursively applied within each subset of the data until a prede-
 235 fined stopping criterion, such as significance or subsample size, is satisfied. A qualita-
 236 tive example of a single decision tree is given in the supporting information.

237 In the final stage, the random forest aggregates predictions from this ensemble of
 238 trees, thereby enhancing prediction stability and performance. For additional insights
 239 into the algorithm and its implementation, refer to Hothorn et al. (2006) and Hothorn
 240 and Zeileis (2015).

241 The models' response, which indicates the rare presence (1) or very frequent ab-
 242 sence (0) of UL, is sampled equally to ensure a balanced representation of the two classes.
 243 Hence, the predicted probabilities of the random forest models shown in this study are
 244 termed "conditional probability" due to the balanced setup of the model response. To
 245 increase the robustness of the results, 10 different random forest models are used to com-
 246 pute the conditional probability. Each of these random forest models consists of the 549
 247 UL observations associated with the larger-scale meteorological setting and 549 randomly
 248 selected non-UL situations. The results shown in this study are the median of these 10
 249 random forests.

250 3.2 Transfer of the Gaisberg model result to the study area

251 Previous studies by the authors have shown that the random forest models trained
 252 on the Gaisberg Tower perform well when tested on withheld data from the Gaisberg
 253 Tower or when tested on another tower, the Säntis Tower in Switzerland (e.g., Stucke
 254 et al., 2023). In this study, the results from the Gaisberg Tower are transferred to a va-
 255 riety of topographic environments from flat to hilly to complex terrain. The tower-trained
 256 random forest model computes the conditional probability of UL in grid cells of 1 km^2
 257 and 1 hour from the larger-scale meteorological reanalysis data. Whether the resulting
 258 models are reasonable is justified by comparing the predicted conditional probabilities
 259 with LLS-observed lightning at tall objects as described in Sect. 2.

4 Results

The results of the study are presented in three distinct parts. In order to take into account the factors that critically influence lightning at wind turbines according to the current lightning protection standards, the LLS-observed lightning at tall objects is compared with the total lightning activity including DL to ground within the selected study area (Sect. 4.1). Then the influence of the effective height of the objects on the LLS-observed lightning is investigated. The section then proceeds to showcase the application of Gaisberg Tower-trained models to the different subareas, illustrating the modeled risk of UL at objects annually and for each season (see Sect. 4.2). Along with this, the seasonal variations of the modeled risk (Sect. 4.2.1) as well as the seasonal variation in the diurnal cycle of the modeled risk is presented (Sect. 4.2.2). Sect. 4.2.3 examines the performance of the results by quantitatively comparing the modeled outcomes with LLS-observed lightning at tall objects. Following this, Sect. 4.3.1 investigates the meteorological conditions that predominantly contribute to UL at the Gaisberg Tower. Section 4.3.2 explains the resulting modeled risk from the most important meteorological variables that affect UL risk, including how these influential variables vary throughout the seasons. A case study is included to demonstrate the models' predictive behavior and the conditions leading to an increased risk of UL (Sect. 4.3.3).

4.1 LLS-observed lightning at tall objects

As mentioned, current lightning protection standards (IEC 61400-24, 2019) take (i) the physical properties of the structure and (ii) the local annual lightning flash density into account. Considering that the effective height may influence lightning at a tall object according to the standards, panels a and b in Fig. 3 examine the role of effective height on the number of flash-hours for objects with corresponding effective height values.

Panel a shows that the majority of objects have an effective height around 100 m. Panel b shows that objects with higher effective heights are more frequently struck by lightning corroborating previous findings (e.g., Rakov & Uman, 2003; Shindo, 2018). The gap between 425 m and 500 m is likely due to the very few objects in that height range being located in areas with low overall LLS-observed lightning at tall objects (see Fig. 4b). The Gaisberg Tower as computed using the method in Zhou et al. (2010) is in a range between 250 m and 275 m.

The second important factor in assessing the risk of lightning at wind turbines according to the standards is the local annual flash density (Fig. 4a).

Fig. 4a shows that the highest concentration of the total lightning activity is in the southern part of the study area in northern Italy. These hotspots are thought to result from enhanced moisture transport from the Adriatic Sea by the mountain plain circulation, which hits the rising topography and initiates convection. This is consistent with previous studies investigating lightning climatologies in these regions (e.g., Simon & Mayr, 2022; Feudale et al., 2013; Taszarek et al., 2019).

However, panel b in Fig. 4 is in stark contrast to panel a, as the maximum cumulative flash-hours of lightning at tall objects are concentrated in the southwesternmost part of the German subarea and the central region of the same subarea. In addition, the central-eastern and southernmost parts of Switzerland show a significant accumulation of flash-hours. Similarly, panel b in Fig. 4 shows no association with the distribution of objects over the study area in panel a of Fig. 2.

Flash-hours in panel b may have DL to ground in addition to lightning at tall objects within the same hour. To examine the proportion of flash-hours exclusively characterized by lightning at tall objects, panel c examines lightning within a 10 km radius

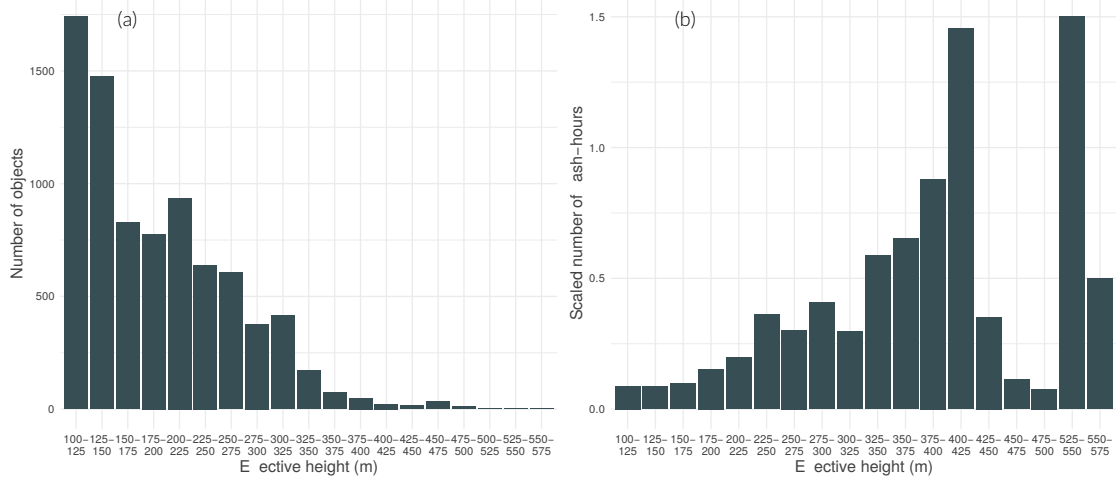


Figure 3: Panel a: number of objects per effective height range. Panel b: number of flash-hours scaled by the number of objects per effective height range.

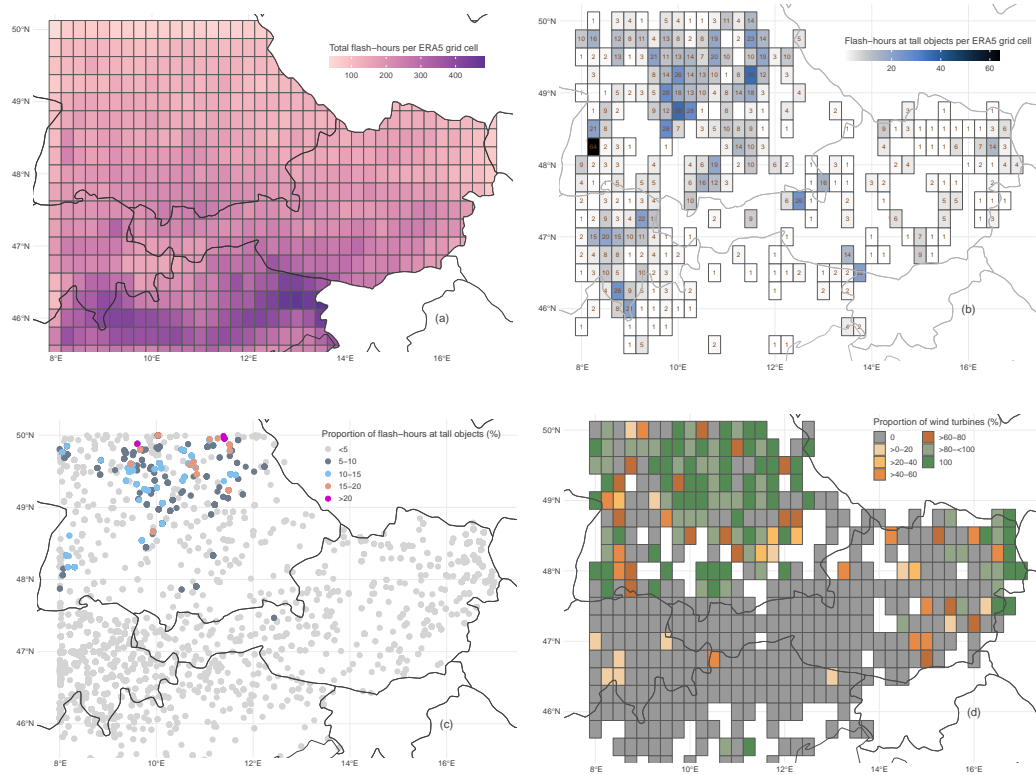


Figure 4: Panel a: total number of flash-hours in ERA5 grid cell (including DL to the ground and lightning at tall objects) between 2021 and 2023. Panel b: accumulated number of flash-hours at objects with effective heights ≥ 100 m. Panel c: proportion of hours exclusively having lightning at tall objects to the total flash-hours 10 km around each object. Excluded are those flash-hours, where also DL to the ground occurred around the object. Panel d: proportion of wind turbines to the total number of objects in cell. One flash-hour is defined by at least one lightning flash within a grid cell and within one hour.

309 of each object. The panel shows that the high concentration of lightning at tall objects
 310 in the Swiss subarea is largely associated with DL to the ground also occurring within
 311 10 km of the tall object within the same hour. In the German subarea, however, the pro-
 312 portion of flash-hours at tall objects with no other lightning activity in the vicinity is
 313 significantly higher than in the other subareas. While in most cases hours with exclu-
 314 sively lightning at tall objects accounts for less than 5 % of the total lightning activity
 315 around a tall object, in the German subarea hours with exclusively lightning at tall ob-
 316 jects accounts for up to 20 % or more of the total. It can be assumed that the mere pres-
 317 ence of the tall object significantly increases the total lightning activity. From Fig. 4d
 318 it can be concluded that lightning at wind turbines accounts for the largest proportion
 319 of lightning activity 10 km around an object in this area, while lightning at wind tur-
 320 bines in the eastern part of Austria, where also many wind turbines are located, accounts
 321 for less than 5% of the surrounding lightning activity.

322 From this analysis it can be suggested that the local flash density does not suffi-
 323 ciently account for the occurrence of lightning at tall objects and in particular for the
 324 occurrence of UL, so that for a more reliable risk assessment detailed meteorological in-
 325 formation must be included.

326 4.2 Modeled risk of UL at tall objects

327 The following analyses highlight the importance of considering the larger-scale me-
 328 teorological environment for accurate UL risk prediction. The figures show the seasonal
 329 variation of the UL risk over the study area as well as the seasonal variation of the di-
 330 urnal cycle of the UL risk. In addition, the predictive performance of the models is pre-
 331 sented and examined seasonally.

332 4.2.1 Seasonal variations of the modeled risk

333 Panels a–d in Fig. 5 depict the risk for fall, spring, summer and winter, while panel
 334 (e) presents the annual risk. Across all five panels, notable regions exhibit increased or
 335 decreased risk of UL according to the larger-scale meteorological setting, and these pat-
 336 terns shift with the seasons. Shown is the modeled seasonal (panels a-d) and annual (panel
 337 e) risk of UL as predicted by the Gaisberg Tower trained random forests, which are solely
 338 based on UL and not DL. Risk is quantified by counting the number of hours in which
 339 the models predict a conditional probability greater than 0.5 for each 1 km² grid cell.
 340 Absolute values of increased risk are difficult to interpret because the tower-trained ran-
 341 dom forests, based on a balanced response with UL and no-UL situations, model the con-
 342 ditional probability.

343 The areas with the highest risk of UL shift throughout the year. From winter through
 344 spring and into summer, the areas of increased risk tend to move both southward and
 345 eastward. In the fall, the region with the highest risk is mainly located in the western
 346 German subarea and the southern German subarea, extending into the Swiss and Aus-
 347 trian northern subareas. While similar in spring, there is a slight southward and east-
 348 ward shift, with the highest risk observed in the westernmost part of Austria extending
 349 eastward through Austria along the Alps, the easternmost part of Switzerland, and the
 350 southwestern part of Germany. In summer, the hotspot regions shift to the eastern and
 351 western parts of northern Italy and the eastern part of Austria. Conversely, in winter,
 352 the highest risk extends over most of the German subarea and the northern parts of Switzer-
 353 land and Austria. In contrast, a rather low risk is observed south of the Alps during the
 354 cold season.

355 Combining the seasonal data reveals a distinct annual pattern (panel e). Areas with
 356 a consistently higher risk include the German subarea, the northern parts of Switzerland

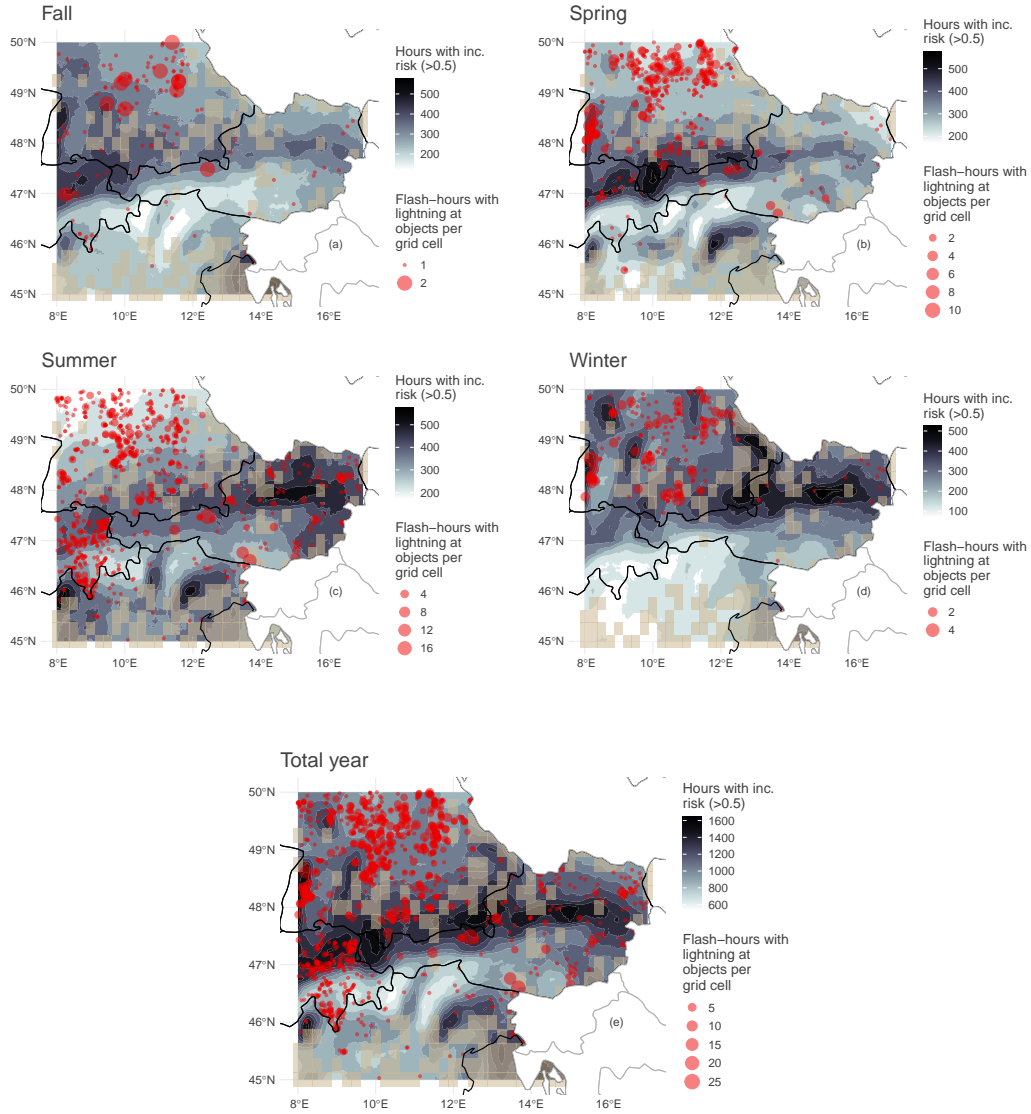


Figure 5: Seasonal (panels a–d) and annual (panel e) UL risk at tall objects modeled by the Gaisberg Tower-trained random forest models. Risk is quantified by counting the number of hours exceeding a conditional probability of 0.5. Red dots are LLS-detected flash-hours at tall objects accumulated to the 1 km^2 grid cell size. The size category numbers are the upper limit, e.g., size category 5 includes flash-hours from 1 to 5. Light beige shaded cells are cells without tall objects.

357 and north western and central Austria, along with the western and eastern parts of north-
 358 ern Italy.

359 Looking at LLS-observed lightning at tall objects possibly including DL at tall ob-
 360 jects and UL (red dots), it is important to note that more than half of the actual UL flashes
 361 may not have been recorded by LLS, as discussed in the introduction. Notably, in win-
 362 ter and the transitional seasons, observed lightning at tall objects is confined to the north-
 363 ern part of the study area, where the highest risk is identified. In contrast, during sum-
 364 mer, observed lightning at tall objects extends to the southern regions, where the risk
 365 is also increased.

366 *4.2.2 Seasonal variations in the diurnal cycle of the modeled risk*

367 Figure 6 panels a–d illustrates that not only does lightning at tall objects vary sea-
 368 sonally, but it also exhibits distinct daily patterns for each season.

369 Notably, despite the common substantial increase in DL activity during the sum-
 370 mer season, the absolute number of flash-hours at tall objects does not vary as much be-
 371 tween seasons as one might expect. The transitional seasons each have a single peak. Ac-
 372 tivity peaks both in the fall and spring around 14 UTC. The most notable difference be-
 373 tween fall and spring is the relatively high activity around midnight in spring, a pattern
 374 also observed in summer. Both the summer and winter seasons have two prominent peaks.
 375 In summer, the first and second peaks occur around 16 UTC and 19 UTC, respectively,
 376 while in winter these peaks occur around 4 UTC and 22 UTC, respectively. This sug-
 377 gests that different meteorological settings may contribute to lightning at tall objects in
 378 different seasons, with strong diurnal heating possibly dominating in summer, trigger-
 379 ing deep convection and other processes, such as those associated with cold fronts, in-
 380 fluencing lightning at tall objects in winter and transitional seasons.

381 The shaded regions in each panel represent the disparity between aggregating hours
 382 with conditional probabilities above 0.25 and those exceeding 0.75. A smaller shaded area
 383 indicates sharper gneiting2007 predictions during observed lightning at tall objects. Con-
 384 trarily, larger shaded areas indicate that the models barely predicted a conditional prob-
 385 ability above 0.75 when lightning was observed at tall objects, indicating less sharpness
 386 in the predictions. Among the four seasons, the predictions in winter are sharpest with
 387 the most narrow shaded areas particularly during nighttime starting from 20 UTC un-
 388 til around 3 UTC. As the random forests model only UL, the best performance in win-
 389 ter might suggest a greater contribution of UL to all lightning at tall objects in the colder
 390 season. Contrarily, the underestimation of random forest models in summer suggests the
 391 dominance of DL in lightning at tall objects which the random forest does not account
 392 for.

393 *4.2.3 Model evaluation*

394 UL is rare resulting in a highly imbalanced dataset with a substantially higher frac-
 395 tion of instances where no UL occurs. To evaluate the performance of the Gaisberg Tower-
 396 trained random forest models in the study area, two statistical approaches are employed.
 397 The basis to understand Fig. 7 is to understand the principle of a confusion matrix ex-
 398 plaining the differences between true/false positives/negatives (see supporting informa-
 399 tion). The performance results are adjusted to fit the ERA5 grid cell size instead of the
 400 original 1 km², which makes it easier to accurately predict lightning at tall objects over
 401 time and space. In these adjusted predictions, only the highest predicted conditional prob-
 402 ability within each ERA5 grid cell is considered.

403 Figure 7a shows the precision-recall curve, selected for its ability to handle imbal-
 404 anced data. In contrast, Figure 7b illustrates the Receiver Operating Characteristic (ROC)
 405 curve, a commonly used method for analyzing model classification performance or to com-

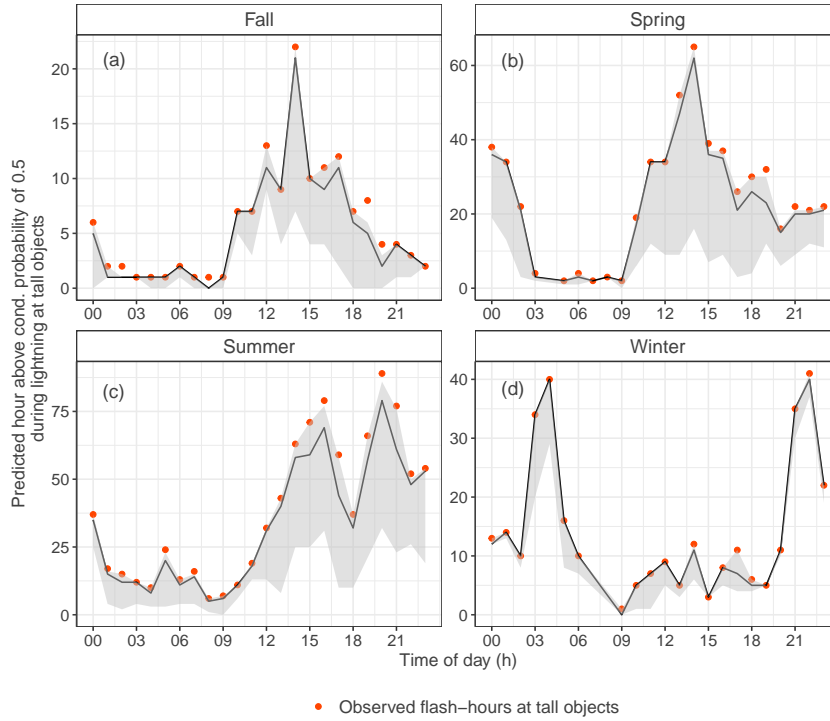


Figure 6: Diurnal cycle of accumulated observed flash-hours at tall objects over the entire study area and verification period (orange dots) versus modeled risk of UL during these events (above conditional probability threshold of 0.5, gray line) of UL. The database consists of LLS-observed lightning at tall objects only and neglects situations without lightning at tall objects. As only hourly predictions are provided, situations in which the same object is hit multiple times within the same hour are only counted once. Shaded area shows the difference of the sum of predicted hours between conditional probabilities of 0.25 and 0.75. Smaller shaded areas indicate sharper predictions for identifying lightning at tall objects. The median values in the predictions for UL at tall objects in winter, summer, fall and spring are 0.834, 0.68, 0.68 and 0.67, respectively.

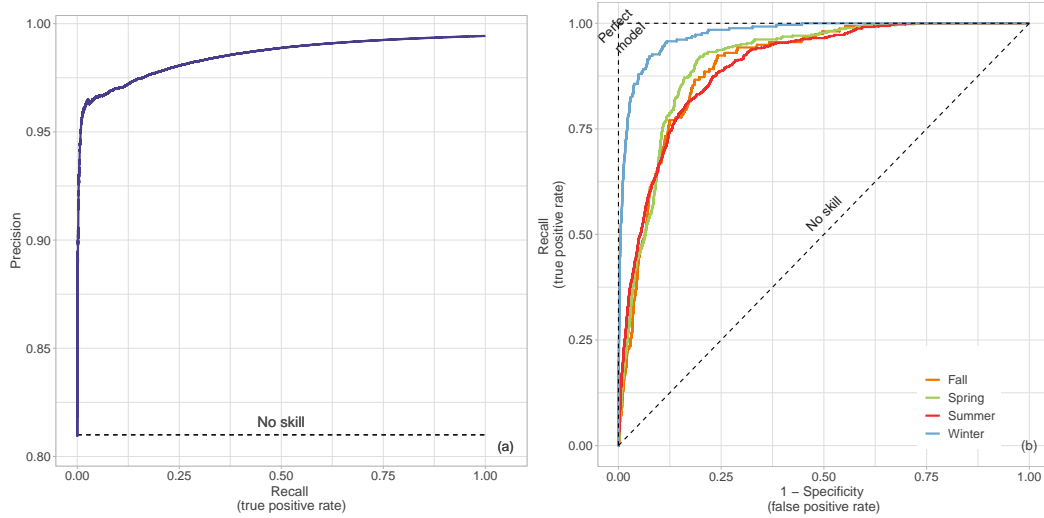


Figure 7: Performance of the random forest models compared to no-skill models. Panel a: precision-recall curve illustrating the trade-off between what proportion of actual UL flashes the model correctly identified (recall), and what proportion of UL flashes predicted by the model actually occurred (precision) for varying cutoff values determining whether UL occurred or not. Panel b: ROC curves for each season showing the trade-off between the proportion with no UL incorrectly predicted as having UL and how well the models predict UL situations that have actually occurred. The larger the area under the curve in both panels, the better the performance.

406 pare different models. For both approaches the area under the curve represents the per-
 407 formance, which increases for larger areas.

408 The precision-recall curve focuses on the positive class, i.e., the UL occurrence and
 409 minority in the data set. It evaluates the relationship between the recall or true posi-
 410 tive rate, i.e., what proportion of actual UL flashes the model correctly identified, and
 411 the precision, i.e., what proportion of UL flashes predicted by the model actually occurred.
 412 The curve shows how precision and recall change at different cutoff values for distinguish-
 413 ing between UL and no UL. In this case, a precision-recall curve that rises rapidly with
 414 increasing recall and levels off slightly in the upper right corner indicates satisfactory model
 415 precision, especially in the early stages of recall. The rapid increase in precision at lower
 416 recall values demonstrates that the models are accurately identifying UL when it actu-
 417 ally occurs, while minimizing the number of actual UL events missed. Seasonally, the
 418 precision-recall curves are almost indistinguishable.

419 Complementing the precision-recall curve, the ROC curve in Figure 7b shows that
 420 the models perform best in winter, as indicated by the blue curve. The ROC curve il-
 421 lustrates the trade-off between how many situations with no UL are incorrectly predicted
 422 as having UL and how well the models predict UL situations that have actually occurred.

423 4.3 The larger-scale meteorological influence on the risk of UL

424 The random forest model takes advantage of information contained in the 35 me-
 425 teorological input variables. It also allows to identify the variables containing most in-
 426 formation about the occurrence of UL.

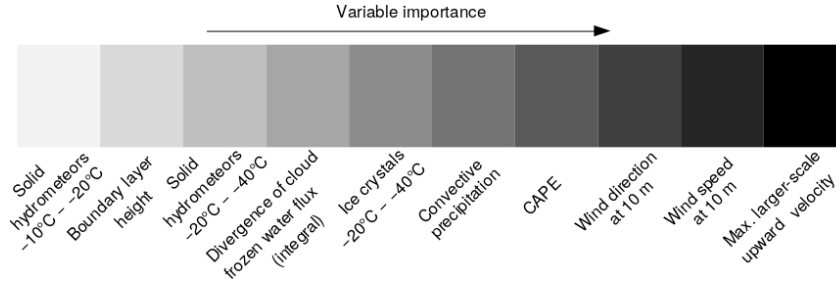


Figure 8: Permutation variable importance according to random forests based on balanced proportions of situations with and without UL at the Gaisberg Tower. Importance increases from left to right.

4.3.1 *The most influential meteorological variables at the Gaisberg Tower*

To calculate the individual impact of each meteorological predictor variable in classifying UL, the values of each predictor variable are randomly shuffled, and the resulting decline in performance is assessed. The larger the decline the more important that variable is.

As evident in the summarized variable importance presented in Fig. 8, one can deduce that both the wind field and cloud physics-related variables exert most influence on the UL occurrence at the Gaisberg Tower, which is in line with earlier research findings (Stucke et al., 2022, 2024). The top five variables include maximum larger-scale upward velocity, 10 m wind speed, 10 m wind direction, convective available potential energy (CAPE), and convective precipitation. Subsequent analyses will specifically focus on the top three most important variables to enhance our understanding of the modeled risk of UL at tall objects. The maximum larger-scale upward velocity should not be confused with the updrafts associated with the convective processes involved in thunderstorm development. Rather, it is the result of larger-scale processes such as lifting along fronts, synoptic troughs or topography.

4.3.2 *Seasonal analysis of the larger-scale meteorology during lightning at tall objects*

Each row in Fig. 9 represents a season and shows a distinct meteorological setting prevalent during LLS-observed lightning at tall objects. The panels summarize the median wind speed and wind direction at 10 m (left column) and the median maximum larger-scale upward velocity (right column).

The increased predicted risk in the German subarea as depicted in Fig. 5 is associated with northerly and northwesterly near-surface winds in all four seasons. Coupled with hilly terrain, where the winds are deflected upward, this causes enhanced larger-scale upward velocities. Consequently, a relatively high risk of UL is evident throughout the year, with the most significant impact observed in the transitional seasons and winter.

Similarly, the increased risk associated with complex terrain appears to result from increased maximum upward velocities, likely induced by strong winds impinging the topography and being deflected upward, triggering convection and UL at tall objects. Depending on the prevailing wind direction, increased larger-scale upward velocities are observed either north or south of the eastern Alps (right column).

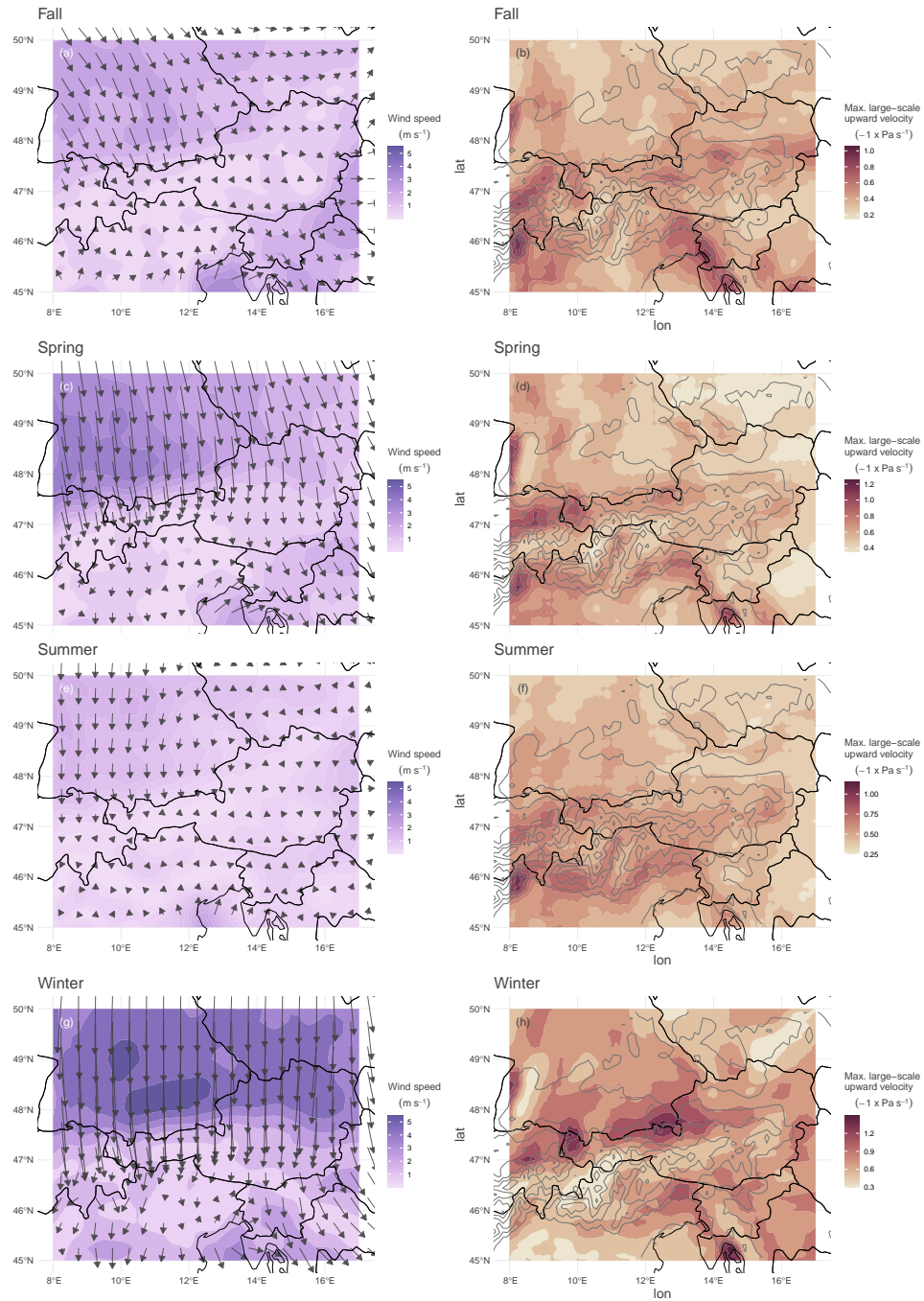


Figure 9: Seasonal median of the three most influential meteorological variables during LLS-observed lightning at tall objects. Left column: wind speed coded by color and wind direction indicated by arrows (average over $0.5^\circ \times 0.5^\circ$). Right column: Median of the maximum larger-scale upward velocity for each season. Negative values indicate upward motion.

Overall, it appears that regions located on the windward side have an increased risk of UL due to comparatively strong near-surface winds and the presence of hills and mountains that deflect the wind upward, creating conditions favorable for UL on tall objects. This is true for the windward side of the northern Alps, which are influenced by strong northerly winds in northern Switzerland, Austria, and the entire German subarea during the transitional seasons and winter. This might also be true for the weak southerly flow, which might influence the risk in western and eastern northern Italy, especially in summer. Conversely, the risk is lower in the central southern Alpine regions of Austria, central southern Switzerland, and central northern Italy.

We propose that especially in winter, and also in spring and fall, processes associated with cyclogenesis, cold front passages, and troughs induce large wind speeds, convective precipitation, and an unstable atmosphere conducive to initiating convection and UL. In contrast, the summer situation might be often characterized by smaller-scale processes and/or strong diurnal heating and solar irradiation, providing conditions for both deep convection initiation and UL at tall objects triggered by nearby DL activity (Stucke et al., 2023).

4.3.3 Case study

A case study of the early morning hours (3–6 UTC) of February 21, 2022 demonstrates the performance of the random forests. For simplicity, again only the three most important meteorological variables out of 35 are examined in detail.

The synoptic situation in this case study is dominated by the passage of a cold front, evident from the densely packed isothermes in panel b. The blue line with triangles illustrates the approximate location of the cold front at 6 UTC after having passed through the north-western corner of the study area. The region with high predicted conditional probabilities is characterized by strong near-surface winds originating from the north, peaking in the area where most actual lightning flashes were observed (panel c). Elevation contour lines in panel a indicate elevated terrain, resulting in increased maximum upward velocity when the wind gets deflected. This, in turn, enhances the probability of UL, particularly in the southwesternmost part of Germany, where actual UL flashes have been observed, as indicated by the yellow dots.

In panel d, a substantial area exceeds a conditional probability value of 0.5, which is the threshold chosen in Fig. 5. The highest predicted probabilities, surpassing 0.8, are concentrated in the German subarea, particularly from western to central southern Germany. Observed lightning at tall objects aligns with the areas of increased risk of UL. However, not all grid cells with elevated probability do experience UL.

5 Discussion

The findings provide clear indications that the seasonal variability in preferred larger-scale meteorological patterns influences the risk of UL at tall objects. Certain regions exhibit higher susceptibility during specific seasons, as also evidenced by observed lightning at tall objects. For instance, in the colder season, the risk is considerably higher north of the Alps. This might be attributed to processes connected to cyclogenesis preferably evolving from north-/north-west to east in the colder season. Conversely, certain areas of northern Italy, particularly the western and eastern parts, where the overall lightning activity is quite high, show a relatively high risk for UL during the summer, in contrast to the lower risk during the colder season. The prevailing favorable meteorological conditions combined with obstructive terrain and elevated effective heights, especially in the hilly regions of southern Germany, may cause the risk to exceed the risk predicted by the random forest models trained on the Gaisberg Tower.

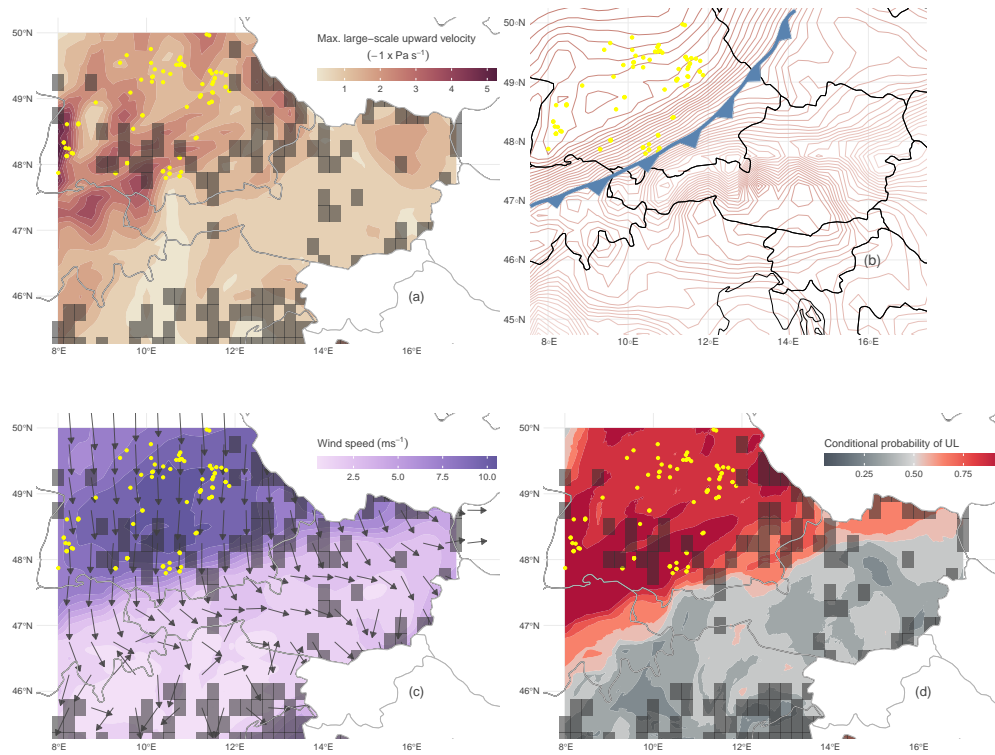


Figure 11: Case study from February 21, 2022 between 3 UTC and 6 UTC. Panel a: maximum of the larger-scale upward velocity over verification period. Panel b: Location of 850 hPa isotherms at 6 UTC with the approximate location of the cold front. Panel c: Color areas are maximum of wind speed over verification period, arrows illustrate wind direction at 6 UTC. Panel d: Maximum of predicted conditional probability over considered verification period. Yellow dots are accumulated LLS-detected flashes at tall structures. Dark gray shaded cells are cells without tall objects.

508 Although observed lightning at tall objects indicate a reasonable risk assessment,
 509 there are naturally discrepancies between the modeled risk and the observation. The most
 510 obvious reason for discrepancies is the fact that the models trained at Gaisberg Tower
 511 consider only UL and ignore DL, since the former is almost exclusively observed at Gais-
 512 berg Tower. While the models only consider UL, lightning at tall objects used for ver-
 513 ification may include both UL and DL, since LLS do not distinguish UL from DL. Con-
 514 sequently, the models may not adequately capture the prevalence of DL at tall objects.
 515 This might be less critical in the winter season, which is suggested to be dominated by
 516 UL (Diendorfer, 2020; Rachidi et al., 2008). Especially in the late afternoon and evening
 517 in summer, the models underestimate the risk of observed lightning at tall objects, while
 518 the increased number of observed lightning at tall objects could actually be majorly DL
 519 at tall objects and not UL striking the object (see Fig. 6).

520 Another aspect is that successful verification depends on the availability of high
 521 quality lightning data. Although the LLS has a high detection efficiency for DL, its ef-
 522 ficiency for UL is less than 50%, which poses a challenge for a reasonable verification of
 523 the modeled risk. Although the models exclude ICC_{only} UL, both ICC_{RS} and especially
 524 ICC_{Pulse} UL also face limitations in detection efficiency (see also Sect. 2).

525 Other non-meteorological factors may significantly influence the occurrence of UL
 526 at wind turbines. Neither topographic characteristics nor varying effective heights can
 527 be accounted for in the tower-trained models. As mentioned, the occurrence of UL at
 528 tall objects is closely related to the effective height, with both UL and DL possible in
 529 the range of approximately 100 m to 500 m. The Gaisberg Tower has a specific effec-
 530 tive height of about 270 m according to Zhou et al. (2010) and considerably higher ac-
 531 cording to Smorgonskiy et al. (2012). Consequently, the maps in Fig. 5 show the risk for
 532 objects in this height range. Figure 3b may be used to adjust it for objects of different
 533 heights.

534 Applying the same algorithm (Zhou et al., 2010) to compute the effective height
 535 as for all other objects, the effective height of Gaisberg Tower is 270 m. Since it sits on
 536 a hill that is approximately 800 m higher than the terrain to the north, its actual effec-
 537 tive height likely exceeds 500 m and was determined (Smorgonskiy et al., 2012) to range
 538 between approximately 300 m to 670 m. From the results we suggest that the combi-
 539 nation of favorable meteorological conditions and increased effective heights, as is espe-
 540 cially the case in southern and southwestern Germany and easternmost Austria, could
 541 increase the fraction of UL over DL in total lightning at tall objects.

542 Physical properties of the object may also play a role, for example, the shape of
 543 the structure, as well as the rotation of the wind turbine blades may affect the UL risk
 544 (Montanyà et al., 2014). In addition, wind farms with many turbines can create "hotspots"
 545 for lightning due to a significant increase in the electric field (Soula et al., 2019). This
 546 would also support the hypothesis that the German subarea, where many wind turbines
 547 are located, has the highest proportion of hours in which only lightning at tall objects
 548 occurs without any other lightning activity to the ground around the turbine.

549 Finally, it is often much more important to correctly predict a high risk at the ap-
 550 propriate time, when the event actually occurs, than to overestimate it. The performance
 551 analysis and verification have shown that the random forest models trained at Gaisberg
 552 Tower are able to reliably and correctly assess this risk, which has the most valuable ap-
 553 plication also for the wind energy sector.

554 6 Conclusions

555 This study examines the risk of lightning at tall objects large enough to experience
 556 a significant proportion of rare but destructive upward lightning (UL). In recent years,
 557 UL has become a major concern for wind turbines as they increasingly suffer from UL.

558 Direct lightning current measurements at the specially instrumented Gaisberg Tower in
 559 Austria show that more than half of the UL is not detected by the local Lightning Lo-
 560 cation System (LLS) due to very specific current waveforms observed in UL making a
 561 proper spatio-temporal risk assessment of UL nearly impossible. Current approaches to
 562 assessing lightning risk often overlook crucial meteorological factors, potentially leading
 563 to a considerable underestimation of UL risk for wind turbines. This study highlights
 564 the necessity of integrating detailed meteorological data into risk assessment to achieve
 565 a more reliable understanding of lightning risk at tall wind turbines.

566 Therefore, this study investigates the larger-scale meteorological role of UL at tall
 567 objects and uses direct UL observations at the Gaisberg Tower together with globally
 568 available larger-scale meteorological reanalysis data. Random forests, a popular and flex-
 569 ible machine learning technique, distinguish UL from non-UL situations. The results show
 570 the importance of wind field and cloud physics relevant variables, which is in agreement
 571 with previous studies. The three most important variables from a set of 35 distinguish-
 572 ing UL from no-UL situations at Gaisberg are the maximum large-scale upward veloc-
 573 ity, wind speed at 10 m, and wind direction at 10 m. Further convective available po-
 574 tential energy and cloud physics related variables are important.

575 In a second step, these findings are applied to a study area covering Austria, parts
 576 of Italy, Germany and Switzerland. The models trained at the Gaisberg Tower predict
 577 the conditional probability of UL within this area at a resolution of 1 km². For verifi-
 578 cation, all objects large enough to experience UL, i.e., having an effective height of ≥ 100
 579 m, are considered, and LLS-detected lightning at tall objects in the verification period
 580 between 2021 and 2023 within a 100 m radius of each tall object are extracted. Tall ob-
 581 jects are distributed throughout the study area, with maxima in the central-eastern Swiss
 582 subarea and eastern Austria. Objects with large effective heights are found in southern,
 583 south-western and central Germany, as well as eastern Austria.

584 The highest LLS-observed activity of lightning at tall objects is mainly in the cen-
 585 tral southern and western German subarea, as well as in the Swiss subarea. Wind tur-
 586 bines are most pronounced in the German subarea and in easternmost Austria. In the
 587 German subarea, lightning at tall wind turbines can account for up to 20 % and more
 588 of the total lightning activity within a 10 km radius particularly around wind turbines.
 589 In all other subareas the proportion of lightning at tall objects to the total lightning ac-
 590 tivity 10 km around an object is less than 5 %.

591 Evaluating the risk of UL at tall objects from Gaisberg Tower-trained random for-
 592 est models based only on larger-scale meteorological variables shows that the annual risk
 593 is highest in southern Germany as well as northern and eastern Austria and northern
 594 Switzerland. Western and eastern northern Italy also have an increased risk of UL. A
 595 seasonal analysis shows that in winter the highest risk is limited to the regions north and
 596 east of the eastern Alps, while south of the eastern Alps (eastern and western northern
 597 Italy) the risk is also increased in the transition seasons and especially in summer. The
 598 analysis of the three main variables shows that the highest predicted probabilities are
 599 due to the deflection of strong larger-scale near-surface winds at the topography, lead-
 600 ing to an increase in larger-scale upward velocities. In the winter and transition seasons,
 601 the wind is predominantly from the north, increasing the risk of UL north of the Alps.
 602 In the warmer seasons and in summer, the increased risk south of the Alps may be due
 603 to other influences, such as thermally driven slope winds, valley winds and mountain-
 604 plain circulations. Between the high-risk areas of southern Switzerland, central north-
 605 ern Italy and southern parts of Austria, the risk is lower in all seasons. The diurnal cy-
 606 cle of the modeled risk varies seasonally. While the transitional seasons show a promi-
 607 nent peak in the afternoon, summer and winter show two prominent peaks. The high-
 608 est risk in summer is in the late afternoon and evening, while the highest risk in win-
 609 ter is in the late evening and night.

610 A comparison with LLS-observed lightning at tall objects shows a qualitatively good
611 agreement with increased or decreased risk. While the areas of increased risk are much
612 larger than areas with observed lightning at tall objects (UL is a very rare phenomenon),
613 the performance of the models to correctly predict high risk of UL when lightning has
614 actually occurred at a tall object is good throughout the year. The precision of the pre-
615 dictions is highest in winter.

616 **Acknowledgements**

617 We acknowledge the funding of this work by the Austrian Climate Research Pro-
618 gram - Implementation (Grant Number: KC305650). The computational results presented
619 have been achieved in part using the Vienna Scientific Cluster (VSC).

620 **Conflict of interest**

621 The authors declare no competing interests.

622 **Data availability**

623 ERA5 data are freely available at the Copernicus Climate Change Service (C3S)
624 Climate Data Store (Hersbach et al., 2020). The results contain modified Copernicus Cli-
625 mate Change Service information (2020). Neither the European Commission nor ECMWF
626 is responsible any use that may be made of the Copernicus information or data it con-
627 tains. EUCLID data and ground truth lightning current measurements from the Gais-
628 berg Tower are available only on request. For more details contact Wolfgang Schulz. The
629 underlying data shown in Fig. 5 can be found in Stucke (2024).

References

630

- 631 Austro Control. (n.d.). *Obstacle data set (ICAO) - austria*. [https://](https://sdimd-free.austrocontrol.at/geonetwork/srv/eng/catalog.search#/metadata/7e38519b-c0c4-4ad3-a918-d38f5f80106b)
632 [sdimd-free.austrocontrol.at/geonetwork/srv/eng/catalog.search#/
633 metadata/7e38519b-c0c4-4ad3-a918-d38f5f80106b](https://sdimd-free.austrocontrol.at/geonetwork/srv/eng/catalog.search#/metadata/7e38519b-c0c4-4ad3-a918-d38f5f80106b). (Accessed: 2024-01-11)
- 634 Becerra, M., Long, M., Schulz, W., & Thottappillil, R. (2018). On the Estimation
635 of the Lightning Incidence to Offshore Wind Farms. *Electric Power Systems
636 Research, 157*, 211–226. Retrieved from [https://www.sciencedirect.com/
637 science/article/pii/S0378779617304790](https://www.sciencedirect.com/science/article/pii/S0378779617304790) doi: 10.1016/j.epsr.2017.12.008
- 638 Birkel, J., Shulzhenko, E., Heidler, F., & Diendorfer, G. (2017). Measuring lightning
639 currents on wind turbines. In *4th International Symposium on Winter Light-
640 ning (ISWL2017)*.
- 641 Breiman, L. (2001). Random forests. *Machine Learning, 45*, 5–32. Retrieved from
642 <https://rdocu.be/c61Vu> doi: 10.1023/A:1010933404324
- 643 Candela Garolera, A., Madsen, S. F., Nissim, M., Myers, J. D., & Holboell, J.
644 (2016). Lightning damage to wind turbine blades from wind farms in
645 the u.s. *IEEE Transactions on Power Delivery, 31*(3), 1043–1049. doi:
646 10.1109/TPWRD.2014.2370682
- 647 Deutsche Flugsicherung. (n.d.). *Obstacle data set - germany*. [https://aip.dfs.de/
648 datasets/](https://aip.dfs.de/datasets/). (Accessed: 2024-01-11)
- 649 Diendorfer, G. (2016). A review of 25 years of lightning research in austria from
650 1991–2015. In *World meeting on lightning*.
- 651 Diendorfer, G. (2020). *Probability of lightning strikes to wind turbines in Eu-
652 rope during winter months* (Tech. Rep.). Copernicus Meetings. doi:
653 10.5194/egusphere-egu2020-3337
- 654 Diendorfer, G., Pichler, H., & Mair, M. (2009). Some parameters of negative
655 upward-initiated lightning to the Gaisberg Tower (2000–2007). *IEEE
656 Transactions on Electromagnetic Compatibility, 51*(3), 443–452. Re-
657 trieved from <https://ieeexplore.ieee.org/document/5089467> doi:
658 10.1109/TEM.2009.2021616
- 659 Diendorfer, G., Pichler, H., & Schulz, W. (2015). LLS detection of upward
660 initiated lightning flashes. In *Proc. 9th asia-pacific international con-
661 ference on lightning (APL)* (p. 5). Nagoya, Japan. Retrieved from
662 [https://www.ove.at/fileadmin/user_upload/aldis/publication/2015/
663 2_APL2015_Diendorfer.pdf](https://www.ove.at/fileadmin/user_upload/aldis/publication/2015/2_APL2015_Diendorfer.pdf)
- 664 Diendorfer, G., Zhou, O.-A., Stockholm, K., & Pichler, H. (2011, 01). Review of
665 10 years of lightning measurement at the Gaisberg Tower in Austria. *Proc. 3rd
666 International Symposium on Winter Lightning*.
- 667 ENAV Group. (n.d.). *Obstacle data set -italy: Aeronautical information publica-
668 tion*. [https://onlineservices.enav.it/enavWebPortalStatic/AIP/AIP/
669 \(A11-23\)_2023.12.28/index.html](https://onlineservices.enav.it/enavWebPortalStatic/AIP/AIP/(A11-23)_2023.12.28/index.html). (Accessed: 2024-02-01)
- 670 Farr, T. G., & Kobrick, M. (2000). Shuttle radar topography mission produces a
671 wealth of data. *Eos, Transactions American Geophysical Union, 81*(48), 583–
672 585.
- 673 Feudale, L., Manzato, A., & Micheletti, S. (2013). A cloud-to-ground lightning cli-
674 matology for north-eastern italy. *Advances in Science and Research, 10*(1), 77–
675 84. doi: 10.5194/asr-10-77-2013
- 676 Hersbach, H., Bell, B., Berrisford, P., Hirahara, S., Horányi, A., Muñoz-Sabater, J.,
677 ... Thépaut, J.-N. (2020). The ERA5 global reanalysis. *Quarterly Journal
678 of the Royal Meteorological Society, 146*(730), 1999–2049. Retrieved from
679 <https://rmets.onlinelibrary.wiley.com/doi/abs/10.1002/qj.3803> doi:
680 10.1002/qj.3803
- 681 Hothorn, T., Hornik, K., & Zeileis, A. (2006). Unbiased recursive partitioning:
682 A conditional inference framework. *Journal of Computational and Graphical
683 Statistics, 15*(3), 651–674. doi: 10.1198/106186006X133933

- 684 Hothorn, T., & Zeileis, A. (2015). partykit: A modular toolkit for recursive party-
685 tioning in R. *Journal of Machine Learning Research*, 16(118), 63905–3909. Re-
686 trieved from <http://jmlr.org/papers/v16/hothorn15a.html>
- 687 IEC 61400-24. (2019). *International standard: Wind energy generation systems -*
688 *part 24: Lightning protection* (Second ed.). Geneva, Switzerland: International
689 Electrotechnical Commission (IEC).
- 690 March, V. (2018). Key issues to define a method of lightning risk assess-
691 ment for wind farms. *Electric Power Systems Research*, 159, 50-57. Re-
692 trieved from [https://www.sciencedirect.com/science/article/pii/](https://www.sciencedirect.com/science/article/pii/S0378779617303450)
693 [S0378779617303450](https://www.sciencedirect.com/science/article/pii/S0378779617303450) (Recent Developments on Lightning Research and Pro-
694 tection Technologies) doi: 10.1016/j.epsr.2017.08.020
- 695 Montanyà, J., Fabró, F., van der Velde, O., March, V., Williams, E. R., Pineda, N.,
696 ... Freijo, M. (2016). Global distribution of winter lightning: A threat to
697 wind turbines and aircraft. *Natural Hazards and Earth System Sciences*, 16(6),
698 1465–1472. Retrieved from [https://www.nat-hazards-earth-syst-sci.net/](https://www.nat-hazards-earth-syst-sci.net/16/1465/2016/nhess-16-1465-2016.pdf)
699 [16/1465/2016/nhess-16-1465-2016.pdf](https://www.nat-hazards-earth-syst-sci.net/16/1465/2016/nhess-16-1465-2016.pdf) doi: 10.5194/nhess-16-1465-2016
- 700 Montanyà, J., van der Velde, O., & Williams, E. R. (2014). Lightning discharges
701 produced by wind turbines. *Journal of Geophysical Research: Atmospheres*,
702 119(3), 1455–1462. Retrieved from [https://agupubs.onlinelibrary.wiley](https://agupubs.onlinelibrary.wiley.com/doi/abs/10.1002/2013JD020225)
703 [.com/doi/abs/10.1002/2013JD020225](https://agupubs.onlinelibrary.wiley.com/doi/abs/10.1002/2013JD020225) doi: 10.1002/2013JD020225
- 704 Pineda, N., Montanyà, J., Salvador, A., van der Velde, O. A., & López, J. A.
705 (2018). Thunderstorm characteristics favouring downward and upward
706 lightning to wind turbines. *Atmospheric Research*, 214, 46-63. doi:
707 10.1016/j.atmosres.2018.07.012
- 708 Rachidi, F., Rubinstein, M., Montanyà, J., Bermudez, J.-L., Sola, R. R., Solà, G., &
709 Korovkin, N. (2008). A review of current issues in lightning protection of new-
710 generation wind-turbine blades. *IEEE Transactions on Industrial Electronics*,
711 55(6), 2489–2496. doi: 10.1109/TIE.2007.896443
- 712 Rakov, V. A., & Uman, M. A. (2003). *Lightning: Physics and effects*. Cambridge
713 University Press. doi: 10.1017/CBO9781107340886
- 714 Schulz, W., Diendorfer, G., Pedebay, S., & Poelman, D. R. (2016). The Eu-
715 ropean lightning location system EUCLID - part 1: Performance analy-
716 sis and validation. *Natural Hazards and Earth System Sciences*, 16(2),
717 595–605. Retrieved from [https://pdfs.semanticscholar.org/dba9/](https://pdfs.semanticscholar.org/dba9/b99d6050e3032b823dc88302fd922b89ab83.pdf)
718 [b99d6050e3032b823dc88302fd922b89ab83.pdf](https://pdfs.semanticscholar.org/dba9/b99d6050e3032b823dc88302fd922b89ab83.pdf) doi: 10.5194/nhess-16-595
719 -2016
- 720 Shindo, T. (2018). Lightning striking characteristics to tall structures. *IEEJ Trans-*
721 *actions on Electrical and Electronic Engineering*, 13(7), 938-947. Retrieved
722 from <https://onlinelibrary.wiley.com/doi/abs/10.1002/tee.22649> doi:
723 <https://doi.org/10.1002/tee.22649>
- 724 Simon, T., & Mayr, G. J. (2022). Lightning climatology for the eastern alpine region
725 on the kilometer scale with daily resolution. *e & i Elektrotechnik und Informa-*
726 *tionstechnik*, 139(3), 352–360. doi: 10.1007/s00502-022-01032-1
- 727 Smorgonskiy, A., Rachidi, F., Rubinstein, M., & Korovkin, N. (2012). On the eval-
728 uation of the effective height of towers: The case of the gaisberg tower. In *2012*
729 *international conference on lightning protection (iclp)* (p. 1-4). doi: 10.1109/
730 ICLP.2012.6344388
- 731 Soula, S., Georgis, J.-F., & Salaün, D. (2019). Quantifying the effect of wind tur-
732 bines on lightning location and characteristics. *Atmospheric Research*, 221,
733 98–110. Retrieved from [https://www.sciencedirect.com/science/article/](https://www.sciencedirect.com/science/article/pii/S0169809518316648)
734 [pii/S0169809518316648](https://www.sciencedirect.com/science/article/pii/S0169809518316648) doi: 10.1016/j.atmosres.2019.01.010
- 735 Strasser, H., & Weber, C. (1999). On the asymptotic theory of permutation statis-
736 tics. *Mathematical Methods of Statistics*, 8, 220-250. Retrieved from [https://](https://epub.wu.ac.at/102/)
737 epub.wu.ac.at/102/
- 738 Stucke, I. (2024). *Spatio-seasonal conditional risk of upward lightning over*

- 739 *the eastern alps, version 2.* Vienna, Austria. CCCA Data Centre.
 740 (<https://data.ccca.ac.at/dataset/spatio-seasonal-conditional-risk-of-upward->
 741 [lightning-over-the-eastern-alps-v02](https://data.ccca.ac.at/dataset/spatio-seasonal-conditional-risk-of-upward-) (accessed April 8, 2024))
- 742 Stucke, I., Morgenstern, D., Diendorfer, G., Mayr, G. J., Pichler, H., Schulz, W.,
 743 ... Zeileis, A. (2022). Thunderstorm types and meteorological characteristics
 744 of upward lightning. In *2022 36th international conference on lightning pro-*
 745 *tection (iclp), 2–7 october 2022, cape town, south africa* (pp. 282–288). doi:
 746 10.1109/ICLP56858.2022.9942489
- 747 Stucke, I., Morgenstern, D., Diendorfer, G., Mayr, G. J., Pichler, H., Schulz, W.,
 748 ... Zeileis, A. (2023). Upward lightning at the Gaisberg Tower: The larger-
 749 scale meteorological influence on the triggering mode and flash type. *Journal*
 750 *of Geophysical Research: Atmospheres*, 128(10), e2022JD037776. Retrieved
 751 from [https://agupubs.onlinelibrary.wiley.com/doi/abs/10.1029/](https://agupubs.onlinelibrary.wiley.com/doi/abs/10.1029/2022JD037776)
 752 [2022JD037776](https://agupubs.onlinelibrary.wiley.com/doi/abs/10.1029/2022JD037776) doi: 10.1029/2022JD037776
- 753 Stucke, I., Morgenstern, D., Diendorfer, G., Mayr, G. J., Pichler, H., Schulz,
 754 W., ... Zeileis, A. (2024). Upward lightning at wind turbines: Risk
 755 assessment from larger-scale meteorology. *Journal of Geophysical Re-*
 756 *search: Atmospheres*, 129(1), e2023JD039505. Retrieved from [https://](https://agupubs.onlinelibrary.wiley.com/doi/abs/10.1029/2023JD039505)
 757 agupubs.onlinelibrary.wiley.com/doi/abs/10.1029/2023JD039505
 758 (e2023JD039505 2023JD039505) doi: <https://doi.org/10.1029/2023JD039505>
- 759 Swiss Federal Spatial Data Infrastructure. (n.d.). *Obstacle data set - switzer-*
 760 *land.* [https://data.geo.admin.ch/browser/index.html#/collections/](https://data.geo.admin.ch/browser/index.html#/collections/ch.bazl.luftfahrthindernis/items/luftfahrthindernis?.asset=asset-luftfahrthindernis_4326.csv.zip)
 761 [ch.bazl.luftfahrthindernis/items/luftfahrthindernis?.asset=asset](https://data.geo.admin.ch/browser/index.html#/collections/ch.bazl.luftfahrthindernis/items/luftfahrthindernis?.asset=asset-luftfahrthindernis_4326.csv.zip)
 762 [-luftfahrthindernis_4326.csv.zip](https://data.geo.admin.ch/browser/index.html#/collections/ch.bazl.luftfahrthindernis/items/luftfahrthindernis?.asset=asset-luftfahrthindernis_4326.csv.zip). (Accessed: 2024-01-11)
- 763 Taszarek, M., Allen, J., Púčík, T., Groenemeijer, P., Czernecki, B., Kolendowicz, L.,
 764 ... Schulz, W. (2019). A climatology of thunderstorms across europe from a
 765 synthesis of multiple data sources. *Journal of Climate*, 32(6), 1813–1837. doi:
 766 10.1175/JCLI-D-18-0372.1
- 767 Vergeiner, C., Schulz, W., & Pack, S. (2013). On the performance of the austrian
 768 lightning detection and information system (aldis). In *Institute of high voltage*
 769 *engineering and system management*. Graz University of Technology.
- 770 Zhou, H., Theethayi, N., Diendorfer, G., Thottappillil, R., & Rakov, V. A. (2010).
 771 On estimation of the effective height of towers on mountaintops in light-
 772 ning incidence studies. *Journal of Electrostatics*, 68(5), 415–418. Re-
 773 trieved from [https://www.sciencedirect.com/science/article/pii/](https://www.sciencedirect.com/science/article/pii/S030438861000077X)
 774 [S030438861000077X](https://www.sciencedirect.com/science/article/pii/S030438861000077X) doi: <https://doi.org/10.1016/j.elstat.2010.05.014>